processes

Article

The Non-Linear Excitation Load-Sharing Method of a High-Powered Nuclear Planetary Gear Train

Fude Wei [1,2], Qingbing Dong [3], Huanhuan Wang [2] and Shuncheng Yang [1,*]

1 Zhengzhou Machinery Research Institute Co., Ltd., Zhengzhou 450001, China; wfdnongda@126.com
2 School of Automotive Engineering, Henan Mechanical and Electrical Vocational College, Zhengzhou 451191, China
3 School of Machinery and Transportation, Chongqing University, Chongqing 400044, China; qdong002@e.ntu.edu.sg
* Correspondence: yangsc@zrime.com.cn

Abstract: The paper primarily employs the 3D calculation method of the helical gear-meshing line and meshing position, in addition to the traditional method of the gear-meshing stiffness calculation. This analysis and correction of load-sharing are beneficial for improving the assembly process of high-powered critical equipment. The dynamic models of rigid–flexible coupling, velocity–torque, and the meshing force of planetary gear trains in nuclear power plants are established based on the principles of gear dynamic characteristics. Based on an analysis of the vibration characteristics of a planetary gear train, a load-sharing method for the planetary gear train is proposed. This uniform load-sharing method is explored under different modification values to provide a reference for load-sharing research on high-powered key equipment. In this paper, a dynamic simulation analysis of the gearbox system is conducted, using virtual prototype software to study the load-sharing performance of the planetary gear system. Furthermore, via a vibration frequency analysis of the gear mesh force, the causes of planetary gear train vibration are discussed, particularly their impact on planetary load. This provides a basis for the assembly process of a nuclear power circulation pump gearbox, ensuring that the gearbox for the circulation pump has a longer life that meets the 40-year service life requirement, and provides a foundation for the study of planetary load characteristics.

Keywords: nuclear gear box; planetary gear train; dynamic characteristics; vibration; load-sharing

Citation: Wei, F.; Dong, Q.; Wang, H.; Yang, S. The Non-Linear Excitation Load-Sharing Method of a High-Powered Nuclear Planetary Gear Train. *Processes* **2023**, *11*, 2190. https://doi.org/10.3390/pr11072190

Academic Editors: Liming Dai and Jialin Tian

Received: 18 May 2023
Revised: 7 July 2023
Accepted: 10 July 2023
Published: 21 July 2023

1. Introduction

The high-powered gear box, which produces over 5000 kW of power, is one of the core devices in the driving system of the circulation pumps that are used in nuclear power plants. It is critical for Chinese companies to develop and master the key technologies in nuclear gear box trains. These technologies help China to improve the localization level of its nuclear power equipment, and it helps to improve the energy security of China [1,2].

The origin of gear dynamics dates back to the 1950s, and since then, the dynamic model of gear systems has gone through a process from a linear model to a complex nonlinear model. Currently, it has developed into a non-linear time-varying model, which covers time-varying mesh stiffness, time-varying gear stiffness, time-varying error excitation, time-varying shock excitation, time-varying backlash, and other factors. Because the nonlinear time-varying model accounts for most factors, it is widely used in current gear dynamics. This paper uses the nonlinear time-varying model. As for its analysis methods, this paper adopts dynamic characteristics research methods, which mainly include the numerical method, analytical method, and experimental method.

Gear internal excitation covers stiffness excitation, error excitation, and shock excitation. The calculation of gear mesh stiffness mainly includes the material mechanics method, finite element method, approximate substitution method, and so on. In gear dynamics modeling, error excitation refers to transmission error excitation. A displacement of the theoretical meshing position of an ideal gear pair with no error and no deformation in the actual meshing position of the driven wheel is defined as a transmission error of the gear [3,4]. Transmission error in gears is the main cause of vibration and noise. Transmission error mainly consists of an elastic deformation of the gear, installation and assembly error, manufacturing error, and profile modification.

Since automatic transmissions require more power combinations than simple planetary gear sets, many researchers have focused on the dynamic characteristics of composite planetary gear sets [5–8]. To date, research on the dynamic behavior of these composite planetary gear sets has been ongoing for a long time [9,10]. During this period, a pure rotational model for the finite configuration of a single-stage composite planetary gear was established, and equations of motion for each configuration were derived. The vibration characteristics were summarized from the numerical results [11]. Based on the pure rotation model mentioned above, the harmonic balance method includes the study of the relationship between the dynamic response and nonlinear errors (such as mesh stiffness, backlash, and transmission errors) [12–14], the pure rotation model of composite planetary gears, and a vibration mode analysis to study the vibration characteristics of its structure [15,16]. Research on the rotation–translation model of general composite planetary gear sets, to characterize the intrinsic relationship of its modes, has subsequently been proposed [17]. In this model, a translation–rotation model, with all its components having translational and rotational vibrations, has been developed to prove that the generally described composite planetary gear system has highly structured modal properties [18,19]. Although many researchers have studied the vibration behavior of composite planetary gear sets, the cited literature confirms that studies investigating the combined effects of internal excitation on the load-sharing behavior of composite planetary gears are limited.

The traditional S-N life curve and strain–life curve methods are only applicable to parts that have regularly structured shapes and are subject to simple loads. For parts with irregularly structured shapes and complex loads, their life can be calculated based on the critical plane method. The critical plane method calculates the damage parameters on all the planes of a certain point of a part and selects the plane with the largest damage parameter as the critical plane for fatigue failure. Substituting the calculated damage parameters of the plane into the corresponding life formula, the life of the specific point can be worked out. In two-dimensional plane strain and plane stress, the normal direction of the critical plane varies from $0°$ to $180°$, while in a three-dimensional analysis, two independent angle variables are required in order to represent the plane normally, and the two angles vary in the range between $0°$ and $180°$. In the numerical calculation, discrete angle values can be used for the damage calculation of a limited number of planes. For an angle increment value of $1°$, 180 planes need to be calculated for the two-dimensional model, and 180×180 planes for the three-dimensional model [20]. Damage parameters include three types: (1) stress; (2) strain; and (3) strain energy density. The critical plane method for different damage parameters is based on the load on the component and the main crack failure type: (1) full shear load parameter, such as shear stress and shear strain, based on crack shapes II and III; (2) full normal force load parameter, such as positive stress and positive strain, based on crack shape I; and (3) mixed load parameter, based on mixed crack shapes.

In the remainder of this paper, Section 2 establishes a dynamic model for nuclear power planetary gears. Section 3 carries out a vibration characteristic analysis of this planetary gear train system. Section 4 carries out a load-sharing analysis of the planetary gear train system. Section 5 discusses the study results. Finally, Section 6 is the conclusion of this paper.

2. Dynamic Characteristics of Planetary Gear Train

This paper conducts a dynamic simulation analysis of the gearbox system by using virtue prototype software and studies the load-sharing performance of the resulting planetary gear system [21]. In addition, through a vibration frequency analysis of the gear meshing force, this study explores the causes of planetary gear train shock. This study mainly adopts a three-dimensional calculation method for the helical gear meshing line and meshing position [22] and a traditional calculation method for the gear meshing stiffness.

2.1. Rigid–Flexible Coupling Dynamic Model of Planetary Gear Train

A planetary gear train is an advanced transmission mechanism that is recognized by having a compact structure, being lightweight, having a small size, a large load-bearing capacity, a large power transmission range, a large transmission range, low noise, a high efficiency, and a long service life. The planetary gear system is composed of a central wheel (sun wheel), a planetary wheel, and a planetary frame. The system rotates about its own axis. The line fixed gear is called the center wheel (also known as the sun wheel). There is a tooth that engages simultaneously with the central wheel and the gear ring, rotating and rotating. There is also a wheel called the planetary wheel. The member supporting the planetary wheel is called the planetary frame.

Due to the complex structure of the gearbox, when the system is running at a high speed, the elastic deformation of each component in the system can have a great impact on the dynamic characteristics of the whole system. Therefore, it is necessary to convert the deformed components in the whole system into flexible bodies for analysis, which can make the simulation results more reliable and accurate. In this paper, transmission gears and planetary racks are converted into corresponding flexible bodies and then a dynamic simulation analysis is carried out.

This paper takes a planetary gearbox (HDBT450) as the research object. The vertical planetary gearbox adopts an NGW (internal and external meshing) structure and is equipped with power four-split herringbone planetary one-stage transmission. The vertical planetary gearbox structure is shown in Figure 1, and the main design parameters are shown in Table 1. Power is transmitted to the sun wheel by the vertical motor through the input gear coupling, and also, power is transmitted to the output shaft through the planetary frame after the planetary star deceleration. Then, the output shaft starts the pump impeller rotation through a coupling connected to it to realize its pumping function.

The structure of the gear box is very complex. When the gear train is running at a high speed, the elastic deformation of each component has a huge impact on the dynamic characteristics of the entire system. Thus, it is necessary to convert the deformed components of the whole system into flexible bodies for analysis to ensure the reliability and accuracy of the simulation model. This paper converts the gears and planet carriers at all levels into corresponding flexible bodies and conducts a dynamic simulation analysis [23].

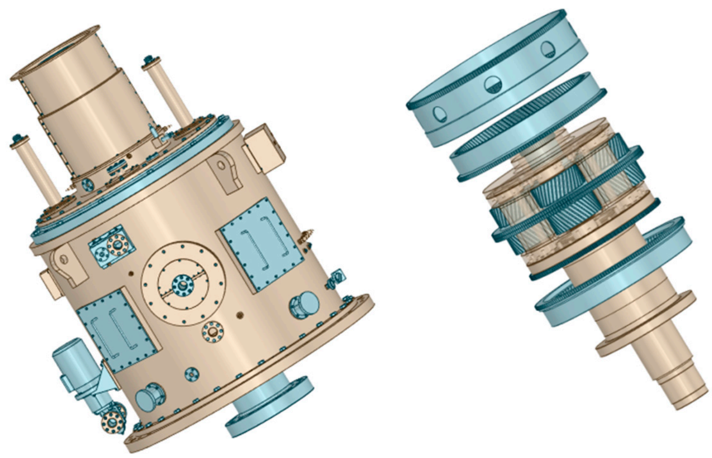

Figure 1. Three-dimensional diagram of the gearbox.

Table 1. Main design parameters of the planetary wheel.

Name	Sun Gear	Planetary Wheel	Inner Gear Ring
Normal module		11 mm	
Number of teeth	35	36	109
Displacement factor	0.3861	0.3940	−0.0403
Tooth breadth (b)	460 mm	460 mm	460 mm
Aperture (d)	200 mm	250 mm	-
Tooth profile angle		20°	
Helical angle		25°	
Tooth top height factor		1.0	
Coefficient of top clearance		0.25	
Young's modulus		206 GPa	
Poisson's ratio		0.3	
Planetary frame torque		373,925.731 N·m	

This paper uses the finite element software Abaqus to establish the corresponding modal neutral file (MNF) of each component in the system, and then import them into ADAMS (automatic dynamic analysis of mechanical systems). The MNF is a stand-alone binary that is unrelated to the actual platform. In addition, the MNF can be exchanged among each system. The establishment of an MNF consists of the following procedures:

(1) Importing the data of the flexible structure components into the Abaqus;

(2) Setting the element type definition and member material properties (elastic modulus, Poisson ratio, and density, etc.);

(3) Mesh generation;

(4) Establishing a rigid connection area;

(5) A modal analysis;

(6) Generating the modal neutral file (MNF).

When the above procedures are completed, the MNF (generated from Abaqus) is imported via the ADAMS data interface, replacing the rigid structural components that need flexibilization, and then the accuracy of the flexible bodies is checked. Before the MNF is imported, all the added constrains are cancelled in relation to the components that need flexibilization. After the MNF is imported, the constrains are added onto the components that need flexibilization and the creation of the rigid–flexible coupling model of the entire system is finished [24].

2.2. Speed and Torque Analysis of Planetary Gear Train

When the above procedures are finished, the model is run in ADAMS and the dynamic simulation is conducted; the rotating speeds of the ring carrier, sun gear, and planetary gear at all levels of the entire transmission system in the post-processing are worked out, and then the transfer of motion among the components of the entire system is studied. The rotating speeds of the ring carrier, sun gear, and planetary gear are shown in Figure 2.

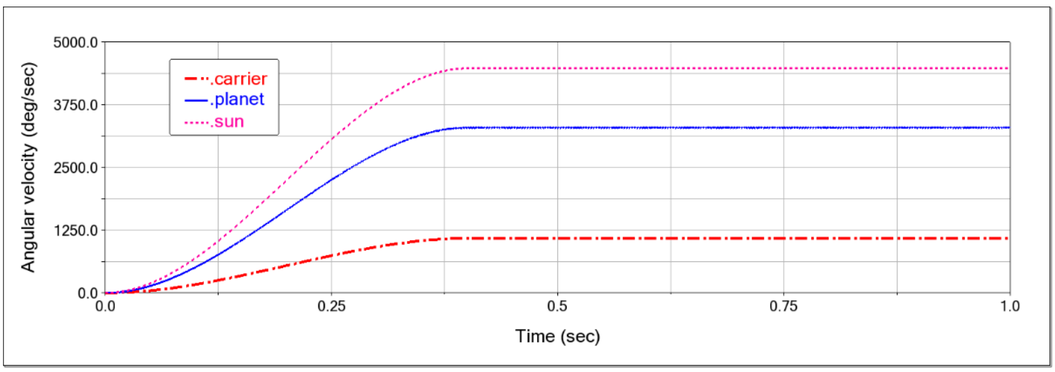

Figure 2. Speed change curve of components in planetary gear train.

It can be seen from Figure 1 that, when the gear train is running, from 0 to 0.4 s, the rotating speed of every component increases slowly from 0 and reaches a relatively stable state at 0.4 s. The reason for such a speed change is incurred by the starting time of the entire system.

From 0.4 s to 1.0 s, the rotating speed of the planetary gear fluctuates periodically up and down near a certain stable value. The reason for this periodic change is caused by a periodic change in the meshing stiffness. Table 2 shows the statistical comparison between the simulation's average value and the calculated theoretical value of the rotating speed of the gear train components at all levels [25].

Table 2. Simulation average value vs. theoretical value of rotating speed of each component in planetary gear train.

	Theoretical Value (N/m)	Simulation Value (N/m)	Error (%)
Sun	4476	4476	0
Planetary	3294.08	3294.2	0.03
Carrier	1087.8	1087.91	0.01

The torque on each component in the gear train is shown in Figure 2.

It can be seen from Figure 3 that, when the gear train is running, from 0 to 0.4 s, the torque on each component increases slowly from 0 and reaches a relatively stable state at 0.4 s. The reason for such a torque change is incurred by the starting time of the entire system.

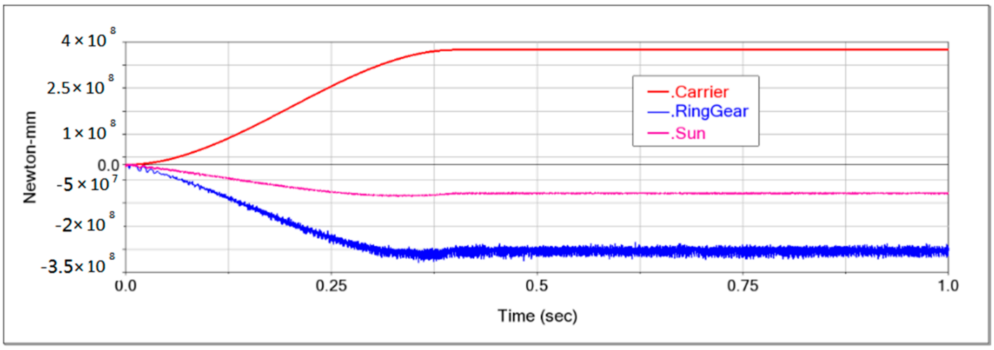

Figure 3. Torque change curve of each component in planetary gear train.

From 0.4 s to 1.0 s, the torque on each component fluctuates periodically up and down near a certain stable value. Table 3 shows the statistical comparison between the simulation's average value and the calculated theoretical value of the torque on each component at all levels.

Table 3. Simulation average value vs. theoretical value of torque on each component in planetary gear train.

	Theoretical Value(N/m)	Simulation Value(N/m)	Error (%)
Sun	90,884.7	92,753	2.05
Ring Gear	283,041.0	280,410	0.93
Carrier	373,925.73	373,925.73	0

Based on the analyses of Figures 2 and 3 and Tables 2 and 3, it is shown that the simulation's average values of the speed and torque of each component are almost the same as those of the theoretical values. This proves that the entire model is correct and that

ADAMS virtual prototype technology is reliable for analyses and research on planetary gear trains. Furthermore, it provides a theoretical basis for further research on the load-sharing characteristics of planetary gear trains [26–29].

2.3. Meshing Force Analysis of Planetary Gear Train

The dynamic simulation is run on ADAMS and the inner and outer meshing force curves are obtained from the post-processor interface. Based on these curves, our team explores the force transmission among the components of the whole planetary gear train system. The following Figures 4 and 5 are generated from the ADAMS postprocessor, showing the meshing force on the inner and outer meshing pair of each planet gear.

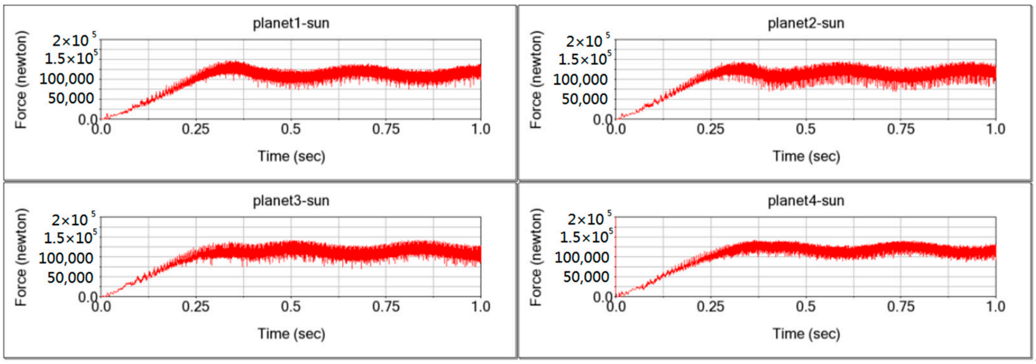

Figure 4. Variation curve of meshing force of each planetary gear in the outer meshing pair of planetary gears.

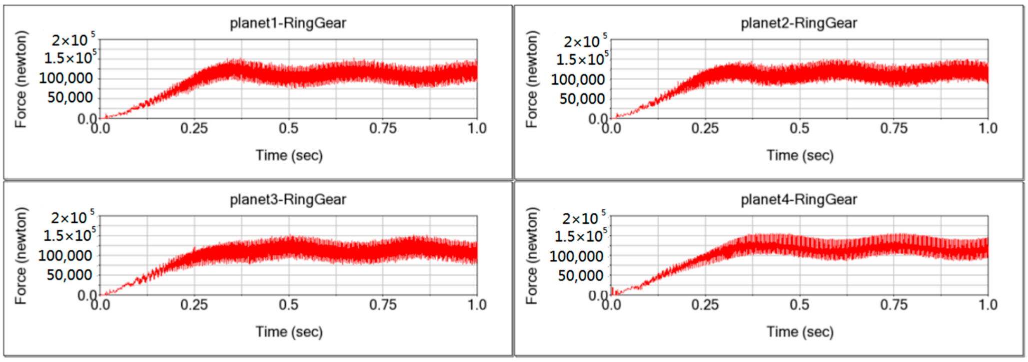

Figure 5. Variation curve of meshing force of each planetary gear in the inner meshing pair of planetary gears.

It can be seen from Figure 3 that, when the gear train is running, from 0 to 0.4 s, the meshing force of each meshing pair increases slowly from 0 and reaches a relatively stable state at 0.4 s. There is a large meshing impact, which is incurred by the starting time of the entire system. During 0.4–1.0 s, each component's speed and the whole gear train system reach a stable status. It can be seen from the images that the meshing force shows a periodic change and fluctuates around a certain stable value.

Through analysis, we find that such a change is caused by a periodic change in the meshing stiffness. The meshing force of each planet gear shows a sinusoidal fluctuation, and the frequency is the same as the rotation frequency of the carrier. Such a phenomenon is caused by the flexible deformation of the ring gear [30–32]. Table 4 shows the average and maximum values of the simulation meshing force in the inner and outer meshing pair of planet gears.

Table 4. Average and maximum value of simulation meshing force in the inner and outer meshing pair of planet gears.

Meshing Pair	Components	Average Value(N)	Max. Value(N)
Inner Meshing	Planet1	1.119×10^5	1.535×10^5
	Planet 2	1.1355×10^5	1.5109×10^5
	Planet 3	1.1393×10^5	1.5311×10^5
	Planet 4	1.1681×10^5	1.5587×10^5
Outer Meshing	Planet 1	1.1304×10^5	1.4004×10^5
	Planet 2	1.1565×10^5	1.4601×10^5
	Planet 3	1.1512×10^5	1.4251×10^5
	Planet 4	1.1709×10^5	1.411×10^5

In mechanical transmission, under ideal conditions, the loads among the planet gears participating in the transmission are evenly distributed and the load values are the same. However, due to the inevitable error caused by the manufacturing process and installation, the planet gears that mesh with the same sun gear bear different loads. Thus, the load-sharing coefficient is used to represent the uniformity of the distributed load of the gear train system. The ideal load-sharing coefficient is 1, and a larger coefficient means that the load-sharing performance of the system is poorer. Let us set the load-sharing coefficients of the inner meshing of each planet gear in each tooth frequency cycle of the system at b_{rpiN}, and the outer meshing at b_{spiN};

$$\left\{\begin{array}{l} b_{\mathrm{spiN}} = \frac{3[F_{spi}(t)]_{\max}}{\sum\limits_{1}^{3}[F_{spi}(t)]_{\max}} \\ b_{\mathrm{piN}} = \frac{3[F_{rpi}(t)]_{\max}}{\sum\limits_{1}^{3}[F_{rpi}(t)]_{\max}} \end{array}\right. \quad t \in [(N-1)T, NT] \tag{1}$$

Then, the inner and outer meshing load-sharing coefficients in the running cycle of the entire gear train system are B_{rpn}, B_{spn}:

$$\left\{\begin{array}{l} B_{spn} = |b_{\mathrm{spiN}} - 1|_{\max} + 1 \\ B_{\mathrm{rp}n} = |b_{\mathrm{piN}} - 1|_{\max} + 1 \end{array}\right. \tag{2}$$

Then, we run a simulation on ADAMS and obtain the meshing force values in the inner and outer meshing pair of each planet gear. Through the above Formulas (1) and (2), the load-sharing coefficient on each stage during the running time of the entire system can be worked out. In the beginning period after starting the system, there is a sharp meshing force change caused by a sudden load upon the system. Thus, we just analyze the meshing force variation during 0.4–1.0 s. Through programming and curving fitting, we obtain the load-sharing coefficient curves of the inner and outer meshing pair on the planet gears at all stages during 0.4–10 s, as shown in below Figures 6 and 7 and Table 5.

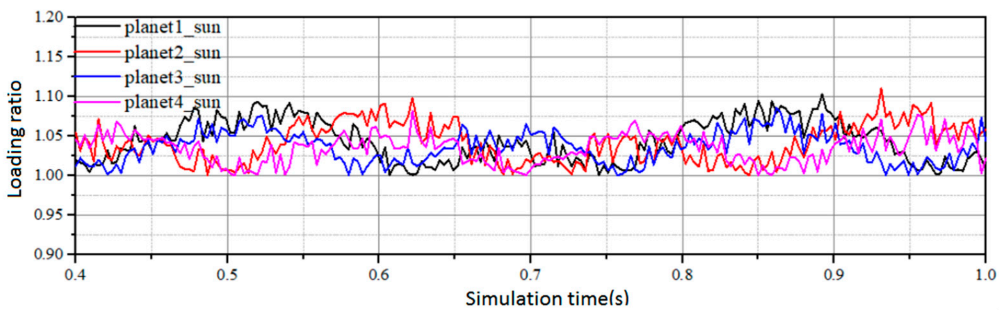

Figure 6. Load-sharing coefficient curve of each planet gears on the outer meshing pair.

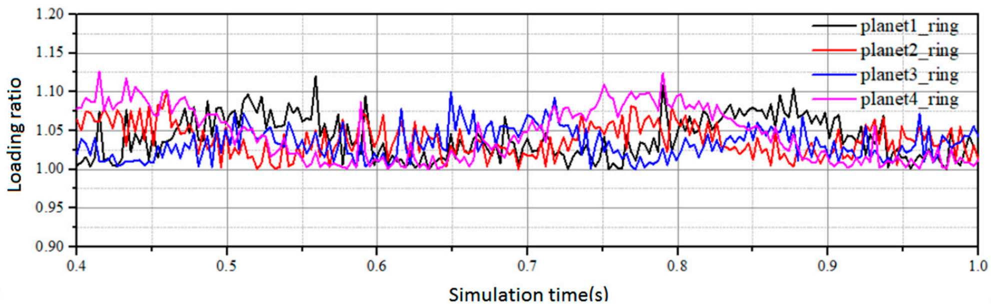

Figure 7. Load-sharing coefficient curve of each planet gears on the inner meshing pair.

Table 5. Load-sharing coefficient in inner and outer meshing pair of planet gears.

Meshing Pair	Components	Load Sharing Coefficient of Components	Load Sharing Coefficient of Meshing Pair
Inner Meshing	Planet 1	1.1204	1.1264
	Planet 2	1.1012	
	Planet 3	1.0996	
	Planet 4	1.1264	
Outer Meshing	Planet 1	1.1025	1.1099
	Planet 2	1.1099	
	Planet 3	1.0859	
	Planet 4	1.0815	

To achieve an even load sharing and ensure the reliability of the system, as well as to extend the system's service life, we need to take measures in the process of the structure design and try to improve the accuracy in the process of the machining and installation of each component, so as to improve the load-sharing performance of the entire planetary gear train system. Generally, measures to improve this load-sharing performance include tolerance control, precise manufacture and installation, floating the load-sharing mechanisms of core components, and an elastic deformation load-sharing technique [33,34]. With regard to the planet gear train model in this paper, we use curved tooth coupling instead of straight tooth coupling. That is because curved tooth coupling has a larger angular displacement, and can compensate for radial displacement, axial displacement, and angular displacement. Curved tooth coupling can also improve the gear tooth contact conditions. Furthermore, curved tooth coupling, recognized by the compact structure, small radius of gyration, heavy load bearing, low noise, high efficiency, and less maintenance, can improve the force transmission efficiency and service life of the planetary gear train system [35]. Therefore, we replace the straight tooth coupling on the sun gear with curved tooth coupling, and make a curve modification on the spline housing connection between the ring gear and its sleeve. By doing so, we make the sun gear and ring gear a floating structure, so as to improve the load-sharing performance of the planetary gear train.

3. Vibration Characteristics Analysis of Planetary Gear Train System

In the process of force transmission, even if the external excitation is 0, system vibration occurs due to a system error and elastic deformation on the gear tooth. In regard to the whole planetary gear train, internal excitation is the key excitation of the system. This paper mainly researches the dynamic characteristics of the entire system under a stable working status and neglects the influence of external excitation on the entire transmission system [36,37]. In the dynamic model, each gear is modeled in an ideal state, and machining errors are not considered. Therefore, in this paper, our research is conducted without a consideration of the error excitation, and we mainly consider the excitation incurred by the time-varying stiffness and meshing impact.

Vibration frequency is the key index for diagnosing and confirming faults in the gear transmission system. For a pair of meshed gears, the main meshing frequency includes the following:

(1) Synchronous speed–frequency

$$f = \frac{n}{60}i \tag{3}$$

In the formula, n refers to the axial speed (r/min); i refers to the frequency harmonic wave, i = 1,2,3. . ., i = 1; and f refers to the fundamental frequency.

(2) Meshing formula of the fixed shaft gear train:

$$f = \frac{nz}{60}i \tag{4}$$

In the formula, z refers to the teeth number; and n refers to the axial speed [38].

(3) Meshing frequency formula for NGW planetary gear train:

$$f = \frac{(n_c \pm n_H)z}{60}i \tag{5}$$

In the formula, nc refers to the planet gear speed, $n_c = (1 - z_b/z_c)n_H$; n_H refers to the carrier speed; Z_b refers to the internal teeth number; and Z_c refers to th eplanet gear teeth number.

We use Formulas (3)–(5) to work out the rotation frequency and mesh frequency of each component in the planet gear train. In the calculation, the rotation frequency of the sun gear is relative to the Earth; the rotation frequency of the planet gear is relative to the carrier; and the rotation frequency of the carrier is relative to the Earth [39]. The data are as shown in Table 6.

Table 6. Rotation frequency and mesh frequency of each component in planetary gear train.

Components	Rotation Frequency (Hz)	Mesh Frequency f_m (Hz)
Sun (f_s)	12.433	329.362
Planet (f_p)	9.150	
Ring Gear (f_r)	0	
Carrier (f_c)	3.022	

The dynamic change in the angular acceleration of the gear transmission reflects the force change of the gear. We explore the vibration frequency of the gear transmission and analyze the angular acceleration of the sun gear and the mechanism of the system vibration [39]. In the research, we export the angular acceleration of the sun gear, conduct Fourier transform on the angular acceleration curve, and obtain the angular acceleration for the frequency domain curve, as shown in below Figure 8. The main peak value of the angular acceleration in the frequency domain curve is 1317.745 Hz, four times the theoretical fundamental meshing frequency of 329.362 Hz, which is worked out according to the formula. The following peak values are three times and two times the theoretical fundamental meshing frequency. From this, we can tell that the vibration frequency of the sun gear mainly contains the fundamental meshing frequency and its harmonic wave, and its main peak value is four times that of the fundamental meshing frequency [40]. The other minor amplitude fluctuation is mainly composed of the rotation frequency of the planet gear fp, the rotation frequency of the sun gear fs, and the rotation frequency of the carrier and their harmonic waves.

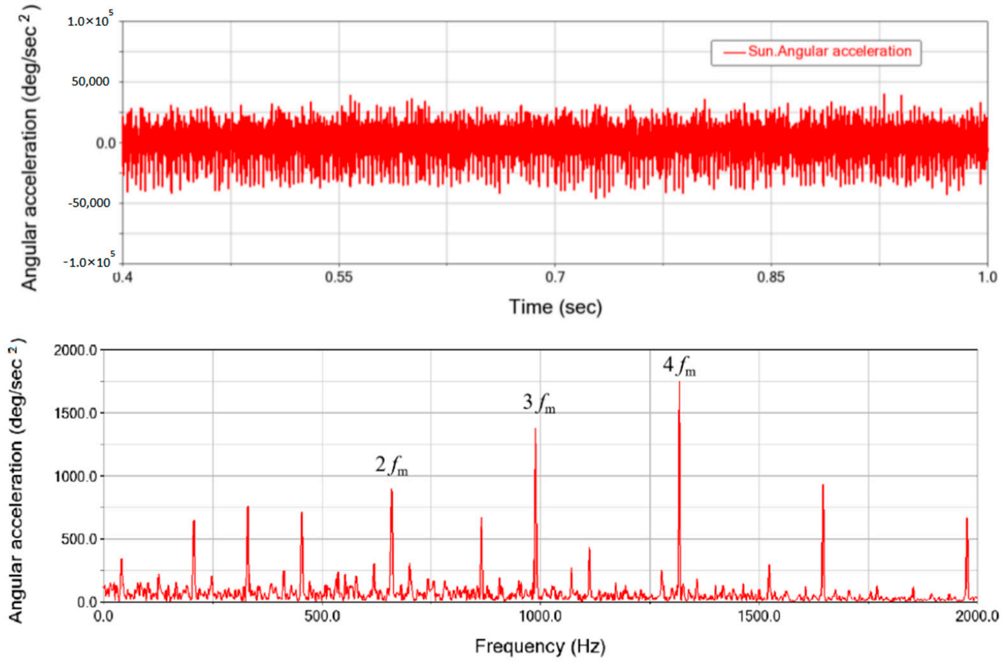

Figure 8. Angular acceleration variation curve and Fourier transform.

We extract the inner and outer meshing component forces of the gear transmission system, then analyze and obtain their values, as well as the reason for the vibration, as shown below in Figures 9 and 10. From these figures in the x, y directions, the vibration mechanisms of the inner and outer meshing forces are the same. In general, these meshing forces show sinusoidal waves, and the wave frequency is the same as the rotation frequency of the carrier [41,42]. Meanwhile, high-frequency vibrations partially occur with time eclipsing. While in the z direction, the meshing force fluctuates around zero, because the double helical gear is symmetrical and the axial forces of the upper and lower gears cancel each other out.

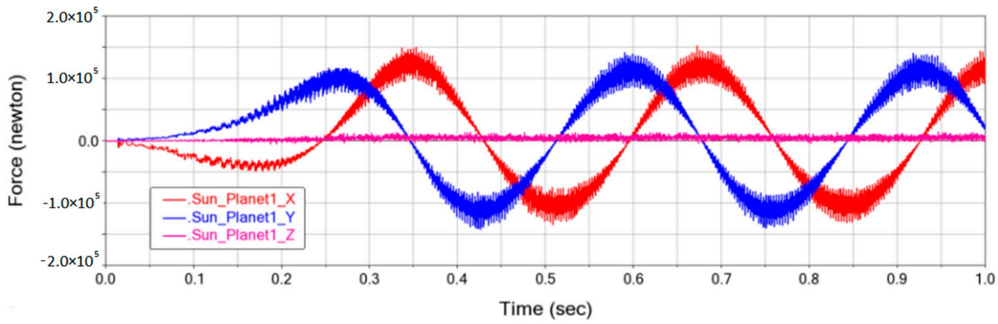

Figure 9. Meshing component force curve of sun gear and planet gear 1.

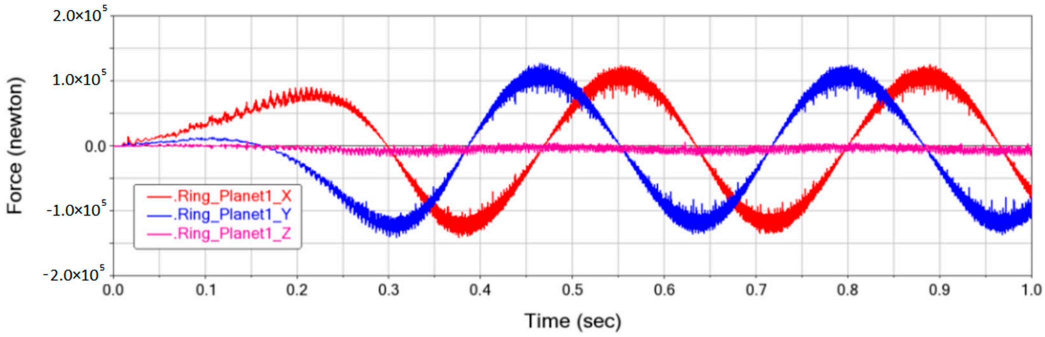

Figure 10. Meshing component force curve of ring gear and planet gear 1.

As shown in Figures 11 and 12, we conduct Fourier transform between the meshing forces in the x and z directions of the sun gear and planet gear 1. Figure 12 shows the meshing force frequency domain curve in the x direction. It also indicates that the main peak value is the rotation frequency of the carrier, and it incurs the meshing force that sinusoidally fluctuates in the x direction, as shown in Figure 9, while the partial high-frequency vibration is mainly caused by the sum/difference value between the meshing frequency, its multiplier, and the rotation frequency of the carrier. In the vicinity of each peak, there is a longer sideband. This is because a sideband consists of many frequencies, including the mesh frequency and its multiplier, and the rotation frequency of each component and their multipliers. These frequencies have research value, such as a working state diagnosis, resonance point identification, and the dynamic vibration reduction design of a gear transmission system [43,44], and these can be used to diagnose the working states of the carrier, planet shaft, and gear. Figure 11 shows the meshing force frequency domain curve of the sun gear and planet gear 1 in the z direction. Figure 11 indicates that the main peak value is the meshing frequency, and the sub peak values are the multipliers of this meshing frequency. The other side-band frequencies are also incurred by the rotation frequency and their multipliers of each component of the planetary gear train system.

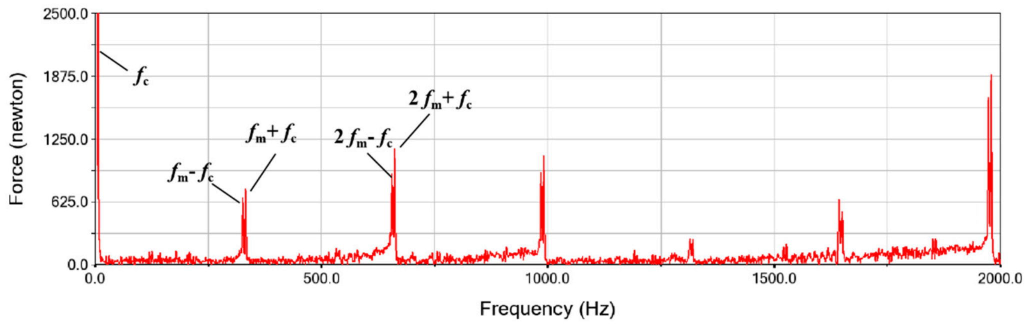

Figure 11. Meshing force frequency domain curve of sun gear and planet gear 1 in x direction.

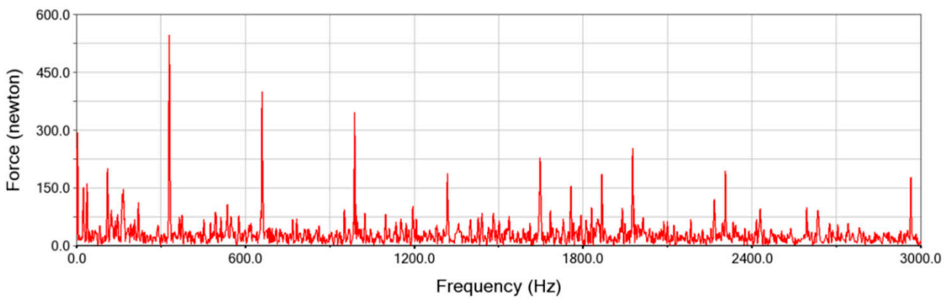

Figure 12. Meshing force frequency domain curve of sun gear and planet gear 1 in z direction.

4. Load Sharing Analysis of Planetary Gear Train System

4.1. Load Distribution

Formula (6) is used to work out the load vibration of a single gear pair in one cycle.

$$F_i = F \times Ratio \tag{6}$$

It can be seen from the analysis that the contact degree of the inner meshing gear pair is 3.6891. At one time, three pairs of gears are in the meshing state, and at one time, four pairs of teeth are in the meshing state. Therefore, in the analysis of a specific pair of teeth, from engagement to exiting the engagement process, at least seven pairs of teeth are required. In this model, nine pairs of teeth are used to study the change in the contact torque during the engagement of the fourth pair of teeth. The global gear model is shown in Figure 13. A mesh refinement was carried out in the contact area. The mesh far away from the contact area was rough, and the cell type was C3D8R. The mesh size of the contact area is about 0.3* ×0.1 × 1.8 mm, the number of tooth ring units is 231,485, and the number of planetary wheel units is 223,579.

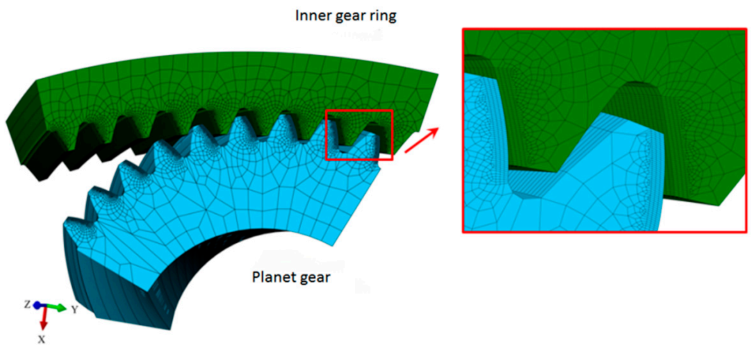

Figure 13. Finite element model of contact between inner gear ring and planetary wheel.

From the above analysis, the contact degree of the outer meshing gear pair is 3.599. In this model, nine pairs of teeth are used to study the change in the contact torque of the fifth pair of teeth during the meshing process. The global gear model is shown in Figures 13 and 14. A mesh refinement was carried out in the contact area. The mesh far away from the contact area was rough, and the cell type was C3D8R. A contact pair is arranged between the sun wheel and the planet wheel tooth surface. The sun wheel tooth surface is the main plane, the planet wheel tooth surface is the slave plane, and the friction coefficient is 0.05. The mesh size of the contact area is about 0.5 * × 1 * × 3 mm, the number of solar wheel units is 206,830, and the number of planetary wheel units is 205,489. The torque to the z axis is applied at the reference point of the ring gear: 35,380.1 N·m. The torque about the z axis is applied at the reference point of the planetary wheel: 11,361 N·m.

In the formula, Fi refers to the load on gear Pair i; F refers to the total normal force; and Ration refers to the load-sharing rations of gear Pair i. Figures 15 and 16 show the stiffness-based inner and outer meshing load-sharing ratios calculated according to the model addendum modification parameters. The red curve is the load-sharing ratio calculated by the model programming of the gear after the addendum modification. The green curve is the load-sharing calculation performed using finite element for the actual modified 3D model after the addendum modification.

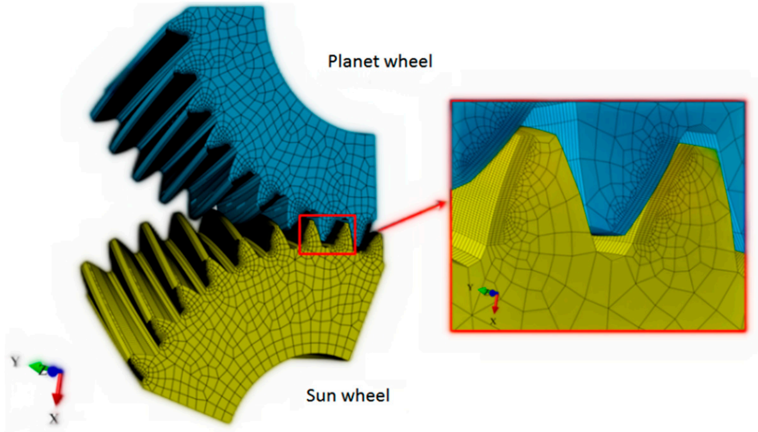

Figure 14. Finite element model of contact between solar and planetary wheels.

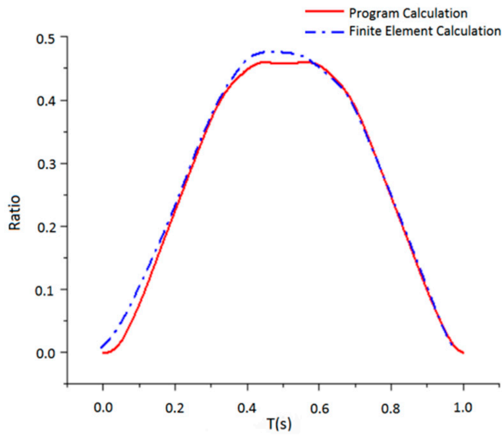

Figure 15. Load-sharing ratio of outer meshing load.

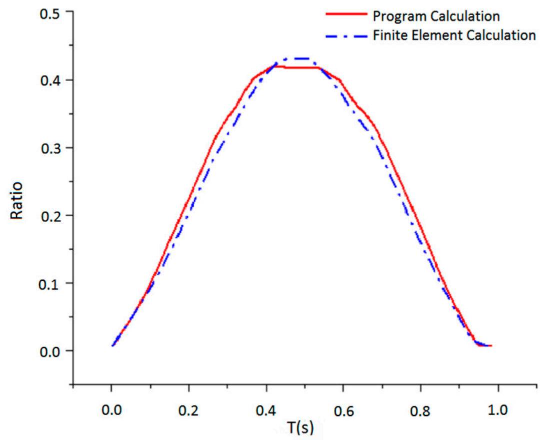

Figure 16. Load-sharing ratio of inner meshing load.

It can be seen from Figures 15 and 16 that the program calculation results are highly consistent with the finite element calculation results, and it proves the correctness of the program calculation. Meanwhile, the program calculation helps to save time significantly [45].

4.2. Influence of Tip Relief Amount on Load Sharing

This paper explores the influence of the tip relief amount and tip relief length on the load sharing of the outer meshing. Figure 17a shows the tip relief amount and Figure 17b shows the relief length. Figure 17a,b indicate that, with an increase in the tip relief amount, the load variation becomes smoother. At the early and late stages, the load becomes smaller. The reason for is that, after tip relief, many gear teeth are no longer engaged in the meshing during this time. In the early–mid stage and mid–late stage of the meshing of one gear tooth pair, the other tooth pairs are either in the early meshing stage or the late meshing stage. This also results in an increase in the load in the early–mid and mid–late stages, and load decreasing in the mid stage. A single tooth (helical) on one side of the outer meshing on the double helical planetary gear can bear a 29,641 N load at maximum.

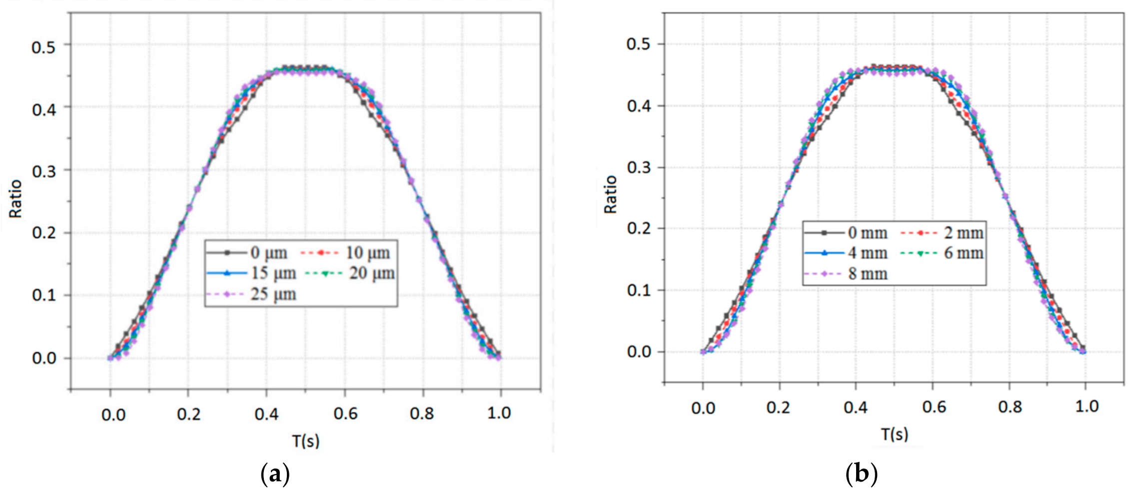

Figure 17. Influence of tip relief amount on load-sharing ratio of outer meshing.

This paper explores the influence of the tip relief amount and length on the load sharing of the inner meshing. Figure 18a shows the tip relief amount and Figure 18b shows the tip relief length. Figure 18a,b indicate that, with an increase in the tip relief amount, the load on a single tooth becomes bigger at an early stage and smaller at a later stage. The reason for this is that, after the tip relief amount, during the meshing time, the load on the modification point on the teeth tip of the planet gear becomes smaller. During the meshing time without tip relief, the load becomes bigger. A single tooth (helical) on one side of the inner meshing on the double helical planetary gear can bear 28,666 N load at maximum.

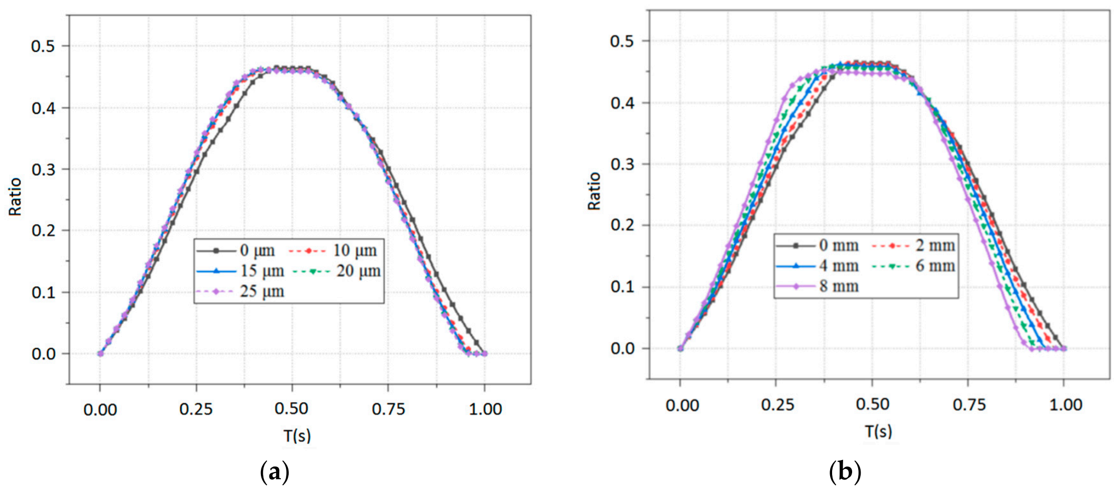

Figure 18. Influence of tip relief amount on load-sharing ratio of inner meshing.

5. Discussion

The internal and external meshing force curves of the planetary gear were calculated to study the power transmission between the various components in the whole planetary gear system. The meshing forces of the internal and external meshing pairs of each planetary gear in the planetary gear system were extracted, respectively. The meshing force showed periodic changes and fluctuated around a certain stable value, which reflects the constant biting in and out of the gear teeth during the meshing process due to periodic changes in the meshing stiffness.

Through data fitting, the average load coefficient of each planetary wheel inner and outer meshing pair in a period of time were obtained. The average load coefficients of the inner and outer meshing were 1.1264 and 1.1099, respectively. In order to improve the load-balancing performance of the system, the sun gear straight gear coupling could be changed to a drum gear coupling, and the spline connection between the gear ring and gear trap could also become a drum-shaped modification. This drum gear coupling could allow for relatively large angular displacement, compensate for the displacement in the radial direction, the displacement in the axial direction, and the angular displacement, and improve the contact conditions between the gear teeth. In this way, the solar wheel and gear ring would become floating components and then improve the load-balancing performance of the system.

6. Conclusions

(1) This paper obtained the variation law of a single time-varying contact line and total time-varying line in the outer meshing in one cycle. That is, in one meshing cycle, the single time-varying contact line increased linearly at first, then held and decreased. The total time-varying contact line showed periodic changes in one cycle, and the number of cycles was related to the gear coincidence. The outer meshing coincidence of the planet gear was 3.599 and the inner meshing coincidence was 3.6189. The maximum length of a single meshing line in the outer meshing (between the sun gear and planet gear) was approximately 125 mm and the maximum length of the total meshing line was 286.5 mm. The maximum length of a single meshing line in the inner meshing (between the planet gear and ring gear) was approximately 131 mm and the maximum length of the total meshing line was 297 mm.

(2) By analyzing the gear meshing stiffness before and after tip relief, we found that, in one meshing cycle, the comprehensive meshing stiffness change trend of the inner and outer meshed gear was consistent with that of the length of the total meshing line. Before the tip relief, the meshing stiffness of the alternating area of the helical gear had a sudden change. With an increase in the tip relief amount, the stiffness change became smooth and the maximum stiffness area in the single-teeth meshing increased gradually. The comprehensive meshing stiffness and three-teeth meshing area increased with an increase in the tip relief amount. A change in the tip relief length had a greater influence on the stiffness value. The meshing stiffness of a single tooth was reduced significantly with an increase in the tip relief length and the change in the comprehensive stiffness in the teeth alternating area became smooth.

(3) The simulation average speed and torque of the whole planetary gear train were not much different from the theoretical value, which verifies the correctness of the whole model and the reliability of the research and analysis when using ADAMS virtual prototype technology, providing a basis for the design and research of load-sharing characteristics in the next step.

Author Contributions: The preliminary investigation, data collection and preparation, data analysis and other work were mainly completed by F.W. and Q.D. provided strong support, and H.W. carried out the computational visualization work. F.W. was responsible for writing and editing the first draft, and Q.D. was responsible for supervision. S.Y. managed the project and provided financial access. All authors have read and agreed to the published version of the manuscript.

Funding: This study was supported by the National Key R&D Program of China (No. 2020YFB2010102).

Data Availability Statement: The data presented in this study are available on request from the corresponding author.

Conflicts of Interest: The authors declare no conflict of interest.

References

1. Lu, C.S.; Wang, X.S.; Leng, X. Investigation on the load sharing characteristic of a two-stage planetary transmission system involving relative floating between stages. *J. Vib. Shock* **2021**, *77–84*, 99.
2. Chen, Y.; Li, J.K.; Zang, L.B. Dynamic simulation and experimental identification for fatigue pitting helical gear fault. *J. Mech. Eng.* **2021**, *57*, 61–70.
3. Wang, Z.H.; Feng, F.Z.; Cong, H. Rigid-flexible coupling modeling and fault characteristic simulation research of planetary transmission system. *J. Mech. Transm.* **2021**, *45*, 46–51.
4. Fan, Z.F. Dynamic characteristics analysis of planetary gear system with pitting failure. *Mach. Tool Hydraul.* **2020**, *48*, 214–217, 223.
5. Zhang, X.H.; Kang, J.S.; Xiao, L. Alpha stable distribution based morphological filter for bearing and gear fault diagnosis in nuclear power plant. *Sci. Technol. Nucl. Install.* **2015**, *2015*, 460131. [CrossRef]
6. Zhang, J.H.; Xiong, X.; He, J. Fault feature extraction for planetary bearing of CRF pump in nuclear power plant based on TFDC-QPSO-optimised MOMEDA. *Meas. Sci. Technol.* **2023**, *34*, 024003. [CrossRef]
7. Struggl, S.; Berbyuk, V.; Johansson, H. Review on wind turbines with focus on drive train system dynamics. *Wind. Energy* **2015**, *18*, 567–590. [CrossRef]
8. Zhang, H.B.; Wu, S.J.; Peng, Z.M. A nonlinear dynamic model for analysis of the combined influences of nonlinear internal excitations on the load sharing behavior of a compound planetary gear set. *Proc. Inst. Mech. Eng. Part C J. Mech. Eng. Sci.* **2016**, *230*, 7–8. [CrossRef]
9. Guo, Y.; Parker, R.G. Dynamic analysis of planetary gears with bearing clearance. *J. Comput. Nonlin. Dyn.* **2012**, *7*, 041002. [CrossRef]
10. Wang, X.S.; Wu, S.J.; Liu, Z.H. Nonlinear dynamic characteristics of compound planetary gear train sets based on harmonic balance method. *Chin. J. Mech. Eng.* **2011**, *1010*, 55–61.
11. Liu, Z.H.; Wu, S.J.; Wang, X.S. Nonlinear dynamics of compound planetary gear sets based on incremental harmonic blance method. *J. Vib. Shock* **2012**, *31*, 117–122.
12. Yyab, A.; Alwidyan, K.; Jawarneh, A. Non-linear dynamic behaviour of compound planetary gear trains: Model formulation and semi-analytical solution. *Proc. IMechE Part K J. Multi-Body Dyn.* **2009**, *223*, 199–210.
13. Shyyab, A.A.; Kahraman, A. A non-linear dynamic model for planetary gear sets. *Proc. Inst. Mech. Eng. Part K J. Multi-Body Dyn.* **2007**, *221*, 567–576. [CrossRef]
14. Boguski, B.; Kahraman, A.; Nishino, T. A new method to measure planet load sharing and sun gear radial orbit of planetary gear sets. *J. Mech. Des.* **2012**, *134*, 071002. [CrossRef]
15. Ye, F.M.; Zhu, R.P.; Bao, H.Y. Dynamic loadsharing behaviors of planetary gear train system with unequal moduli and pressure angles. *J. South China Univ. Technol.* **2011**, *39*, 117–123.
16. Zhou, J.X.; Dong, H. On load sharing characteristic of planetary gear system based on nonlinear dynamics. *Mech. Sci. Technol. Aerosp. Eng.* **2008**, *6*, 026.
17. Al-Shyyab, A.; Kahraman, A. Non-linear dynamic analysis of a multi-mesh gear train using multi-term harmonic balance method: Period-one motions. *J. Sound Vib.* **2005**, *284*, 151–172. [CrossRef]
18. Wang, J.G.; Yang, S.N.; Liu, Y.D. Analysis of load-sharing behavior of the multistage planetary gear train used in wind generators: Effects of random wind load. *Appl. Sci.* **2019**, *9*, 5501. [CrossRef]
19. Zhang, Y.X.; Tu, H.; Lu, J. Simulation research on gear crack fault based on ADAMS. *J. Mech. Strength* **2020**, *42*, 1277–1285.
20. Qiu, X.; Han, Q.; Chu, F. Load-sharing characteristics of planetary gear transmission in horizontal axis wind turbines. *Mech. Mach. Theory* **2015**, *92*, 391–406. [CrossRef]
21. Feng, Z.; Zuo, M.J. Vibration signal models for fault diagnosis of planetary gearboxes. *J. Sound Vib.* **2012**, *331*, 4919–4939. [CrossRef]
22. Zhao, D.; Wang, T.; Chu, F. Deep convolutional neural network based planet bearing fault classification. *Comput. Ind.* **2019**, *107*, 59–66. [CrossRef]
23. Bai, J.L.; Zhao, J.S.; Li, Y.Q. Effect of timing gear phase coefficient on vibration characteristics. *Trans. CSICE* **2020**, *38*, 375–383.
24. Ligata, H.; Kahraman, A.; Singh, A. A closed-form planet load sharing formulation for planetary gear sets using a translational analogy. *J. Mech. Des.* **2009**, *131*, 210071–210077. [CrossRef]
25. Yuan, G.Q.; Li, J.K.; Hu, Y.B. Development and research status of key technology of land gas turbine gearbox in China. *J. Mech. Transm.* **2020**, *44*, 163–170.
26. Li, H.K.; Hou, M.F.; Tang, D.L. Fault diagnosis of low speed gearbox based on POVMD and CAF. *J. Vib. Meas. Diagn.* **2020**, *40*, 35–42.
27. Liu, H.M.; Jiang, J.K.; Liu, Z. Analysis of statics load sharing based on meshing characteristic for straight bevel gear split transmission. *J. Mech. Transm.* **2021**, *45*, 29–33.
28. Lv, S.H.; Li, Z. Influence of star gear support stiffness on load sharing characteristics of two-tage star gear transmission system. *Mach. Build. Autom.* **2021**, *50*, 25–28.
29. Fu, X.Z.; Huang, Y.X.; Fang, Z.D. Static load sharing character Istics of dual branch transmission system with general spur face gears. *J. Huazhong Univ. Sci. Technol.* **2021**, *49*, 64–71.
30. Mark, W.D.; Hines, J.A. Stationary transducer response to planetary-gear vibration excitation with non-uniform planet loading. *Mech. Syst. Signal Process.* **2009**, *23*, 1366–1381. [CrossRef]

31. Wei, W.; Guo, W.Y.; Han, J.G. Load sharing characteristics of dual-input torque-spilt gear system considering stiffness. *J. Natl. Univ. Def. Technol.* **2021**, *43*, 132–140.
32. Jin, G.H.; Gao, P.; Yan, Y.S. Sensitivity analysis of influence of stiffness and backlash on load sharing characteristics of power split drive system. *J. Cent. South Univ.* **2021**, *52*, 1149–1159.
33. Han, J.; Li, W.; Qiao, Z.L. Lubrication characteristics of cycloid pin wheel transmission of RV reducer. *J. Cent. South Univ.* **2021**, *28*, 398–417. [CrossRef]
34. Liu, Z.; Lei, Y.; Liu, H.; Yang, X.; Song, W.L. A phenomenological model for investigating unequal planet load sharing in epicyclic gearboxes. *Mech. Syst. Signal Process.* **2020**, *135*, 106414. [CrossRef]
35. Lei, Y.G.; Liu, Z.Y.; Lin, J.; Lu, F.B. Phenomenological models of vibration signals for condition monitoring and fault diagnosis of epicyclic gearboxes. *J. Sound Vib.* **2016**, *369*, 266–281. [CrossRef]
36. Feng, S.; Zhou, H.Y.; Dong, H.B. Application of deep transfer learning to predicting crystal structures of inorganic substances. *Comput. Mater. Sci.* **2021**, *195*, 110476. [CrossRef]
37. Nenchev, B.; Tao, Q.; Dong, Z.; Panwisawas, C.; Li, H.; Tao, B.; Dong, H. Evaluating data-driven algorithms for predicting mechanical properties with small datasets: A case study on gear steel hardenability. *Int. J. Miner. Metall. Mater.* **2022**, *29*, 836–847. [CrossRef]
38. Du, Y.Y.; Wang, X.S.; Yang, X. Influence of center component floating on the load-sharing characteristic of planetary transmission system. *J. Mech. Transm.* **2019**, *43*, 11–16.
39. Zhang, J.; Chen, T.; Wang, J. Tooth modification of helical planetary gear train based on minimum dynamic transmission error fluctuation. *J. Vib. Shock* **2019**, *38*, 77–88.
40. Chen, F.; Li, C.S. Simulation of mechanical performance for planetary reducer gear based on LMS virtual. *Lab. Coal. Mine Mach.* **2019**, *40*, 157–159.
41. Akinlabi, E.T.; Ikumapayi, O.M.; Bodunde, O.P.; Adara-Mola, B.A.; Uchegbu, I.D.; Fatoba, S.O. Impact of quenching on the hardenability of steels EN-3 (~1015), EN-8 (~1040) and EN-24 (~4340) during Jominy end quench technique. *Int. J. Emerg. Technol.* **2020**, *11*, 290.
42. Brien, E.C.H.C.O.; Yeddu, H.K. Multi-length scale modeling of carburizeation, martensitic microstructure evolution and fatigue properties of steel gears. *J. Mater. Sci. Technol.* **2020**, *14*, 157–165. [CrossRef]
43. Wu, S.J.; Feng, F.Z.; Wu, C.Z. Application of fast kurtosis spectrum in fault feature extraction of compound planetary gear. *J. Mech. Transm.* **2019**, *43*, 151–157.
44. Dong, H.; Liu, Z.Y.; Zhang, J.W. Analysis of static load sharing characteristics of planetary gear transmission system based on clearance floating. *J. Yanshan Univ.* **2019**, *43*, 291–297.
45. Zhang, L.L.; Zhu, R.P. Impact of meshing phase on load sharing for herringbone planetary train. *J. Mech. Eng.* **2018**, *54*, 129–140. [CrossRef]